

# Computational Modeling and Analysis of Biomimetic Flight Mechanisms

R. Mittal<sup>1</sup>, Y. Utturkar<sup>2</sup>, and H.S. Udaykumar<sup>3</sup>

<sup>1</sup>Department of Mechanical and Aerospace Engineering  
The George Washington University  
Washington D.C. 20052

<sup>2</sup>Department of Mechanical Engineering  
University of Florida  
Gainesville, Florida 32611

<sup>3</sup>Department of Mechanical Engineering  
University of Iowa  
Iowa City, Iowa 52242

## ABSTRACT

Numerical simulations have been used to study the fluid dynamics associated with flapping flight modes of single as well as paired wings. The numerical solver employed is based on a sharp-interface, Cartesian grid method that allows us to simulate flow with moving boundaries on stationary Cartesian grids. Here, the simple case of normal hover is examined and the thrust production and vortex dynamics of a single wing undergoing a combined pitch-and-heave maneuver is analyzed. Following this, the fluid flow associated with a paired wing is examined with particular emphasis on the effect of phase lag between the two wings on thrust production and efficiency.

## 1. INTRODUCTION

Current interest in micro-aerial vehicles (MAVs) has been one of the main motivating factors in the recent surge of research activity in the area of insect and bird flight (Ellington 1999). The flow physics of flight at small scales is fundamentally different from conventional wing aerodynamics and much of our existing knowledge base regarding the aerodynamic design of aircrafts is of limited use in the design of MAVs. Since insects and birds have perfected, through millions of years of evolution, the apparatus and technique for achieving flight at these small scales, it seems clear that much could be learned regarding the aerodynamic design of MAVs by analyzing insect and bird flight.

The two key features that distinguish insect and bird flight from conventional airplane flight are the significantly lower Reynolds numbers and the ubiquity of unsteady aerodynamic mechanisms. From the point of view of computational modeling, the former is a blessing since low Reynolds numbers translate to low spatial and temporal resolution requirements.

The latter feature on the other hand, brings with it significant complications since it mandates the inclusion of complex moving boundaries in the computation. Consider for example, the flight of a typical dragonfly shown in Figure 1. The frequency of wing flapping is about 30Hz, the wing chord and total span are about 1cm and 10 cm respectively and the amplitude at mid-span is about 3cm. The Reynolds number based on the wing chord and the maximum wing velocity is therefore about 8000. The dragonfly however has two pairs of wings that do not beat in unison. In fact, in typical flight, the hindwings lead the forewings by phase angles between 50° to 100° (Soms & Luttgies 1985). It is thought that the phase lag between the two wing pairs is chosen so as to gain some aerodynamic advantage and if the underlying flow physics of such a paired wing could be understood, then it could potentially be utilized in the design of MAVs. However, computational modeling of such a paired wing is a non-trivial proposition since the computation would have to include multiple, complex shaped, moving boundaries.

In the computational modeling of such flows, Cartesian grid methods, where the flow is simulated on a non-conformal Cartesian mesh has significant advantages over conventional body-conformal (structure or unstructured) grid methods. In Cartesian grid methods, since the grid does not conform to the body, grid generation and complexity is significantly reduced. This is especially advantageous for simulating flow with moving boundaries since it eliminates complex mesh evolution/motion strategies that typically have to be employed in conventional body-conformal Lagrangian methods.

In the current paper, we describe the use of a recently developed Cartesian grid method for the simulation and analysis of some simple mechanisms associated with the flight

of insects and/or birds. The salient features of the numerical method are described first. This is followed by a discussion of the simulation of two configurations, the first being the combined pitch-and-heave maneuver of a single wing in hover and second, the flow produced by a paired wing.

## 2. FLOW CONFIGURATION AND SIMULATION APPROACH

**Flow Configuration.** Combined pitch and heave (or pitch and plunge) is a primary wing motion through which insects and birds achieve the thrust and lift required for flight. Figure 2 shows this motion for an elliptic airfoil in a freestream (with speed  $U_\infty$ ) and the motion of the moving airfoil may be specified as:

$$\begin{aligned}x_o(t) &= A \cos(\beta) \sin(\omega t); \\y_o(t) &= A \sin(\beta) \sin(\omega t); \\ \alpha(t) &= \alpha_a \cos(\omega t + \phi)\end{aligned}$$

where  $(x_o, y_o)$  is the location of the center of the ellipse and  $\alpha$  is the pitch-angle measured from the normal to the stroke plane which is itself inclined at an angle  $\beta$  with the horizontal. The flow produced by such a flapping foil is governed by the following set of non-dimensional parameters:  $A/c$ ,  $\alpha_a$ ,  $\phi$ ,  $\beta$ ,  $U_\infty / \omega A$  and  $\omega c A / \nu$ , where the last parameter represents a Reynolds number (Re) based on the maximum heave velocity and the airfoil chord. By choosing  $U_\infty / \omega A = \phi = \beta = 0$ , the so-called "normal hovering mode" is obtained. In this mode, the foil moves in a horizontal plane and is oriented vertically at the two ends of the stroke. At the center of the stroke, the foil has an angle of inclination from the vertical equal to  $\alpha_a$  as it moves to the right, and  $-\alpha_a$  as it moves to the left. In this mode, the foil is expected to produce a positive mean vertical (thrust) force and a zero mean horizontal (side) force. This type of hovering mode has been studied previously by Freymuth (1990) and also by Gustafson and Leben (1991) and Wang (2000). However, despite these previous studies, much remains to be explored and understood regarding the flow physics of this simple flapping mode. In the current study of the single wing, a one-eighth thickness ratio elliptic airfoil is employed and parameters  $A/c$  and Re are fixed at 1 and 125 respectively.

**Simulation Approach.** A previously developed Cartesian grid solver is employed in these simulations and details of the solution procedure can be found in Udaykumar et al. (1999) Ye et al. (1999) and Udaykumar et al. (2001). This solver allows simulation of unsteady viscous incompressible flows with complex immersed moving boundaries on Cartesian grids. Thus, the grid does not need to conform to the complex moving boundaries and this simplifies the gridding of the flow domain. The solver employs a second-order accurate central difference scheme for the spatial discretization and a mixed explicit-implicit fractional step scheme for time advancement. An efficient multigrid algorithm is used for solving the pressure Poisson equation.

The key advantage of this solver for the current flow is that the entire geometry of the moving single as well as paired wing is modeled on the stationary Cartesian mesh. As the wing(s) moves over the underlying Cartesian mesh, only the discretization in the cells cut by the solid boundary is modified to account for the presence of the solid boundary.

All results presented here have been obtained on a  $522 \times 452$  mesh on a  $40c \times 40c$  computational domain. Furthermore, the time-step used in the simulations is such that it requires 6250 time-steps to complete one cycle, thereby ensuring high temporal accuracy. "Soft" homogeneous Neumann velocity boundary conditions are used at all outer boundaries and this allows the flow to enter or exit the domain in a natural manner. For pressure, we impose a fixed value at the upper, right and left boundaries. On the lower boundary, where we expect the hover jet to exit, a homogeneous Neumann pressure boundary condition is applied which, together with the soft velocity boundary condition, allows vortex structures to exit the domain with minimal reflection and distortions.

## 3. SIMULATION RESULTS

In this section, we summarize the salient results obtained for both the single and paired wing simulations.

### Single Wing

Figure 3(i) shows a sequence of spanwise vorticity contour plot for the  $\alpha_a = 45^\circ$  simulation and for this case we find that the motion of the foil produces a reverse Karman vortex street. The plots indicate that the process of formation of this type of wake topology is similar to that described by Freymuth (1990). At roughly the middle of the stroke ( $x_o = 0$ ), a strong stall vortex forms on the lee side of the foil. As the foil continues its motion, approaching its maximum excursion and starts to pitch rapidly, the stall vortex moves down the length of the foil and amalgamates with the trailing edge vortex. This combined vortex grows as the airfoil moves to the other end and also convects slightly downwards due to the action of the hover jet created by the airfoil motion. As the foil reaches the other end, the tail of the vortex, which was till that time attached to the trailing edge, gets severed by the stall vortex of opposite sign. With continuing motion of the foil, the severed vortex gets convected further down by the action of the hover jet and this process now repeats for the opposite sign vortex. It is further found that the vortices have a well organized staggered arrangement near the foil but tend to become disorganized further down the hover jet.

Figure 3(ii) show a sequence of vorticity contour plots for  $\alpha_a = 60^\circ$  where the phase for these plots is the same as for the previous case. The plots indicate a markedly different behavior in the evolution of the vortex structures. A street of vortices is observed to form, however, this street is not as well organized as that for  $\alpha_a = 45^\circ$  and furthermore, there is clear asymmetry in the flow about  $x=0$ . In particular, it is found that counter-rotating vortices pair up and drift towards the right of the centerline. On closer examination it is found that, the difference

is due to the formation of a small but distinct trailing edge vortex. This vortex affects the evolution of the subsequent vortex and prevents the vortices from aligning in an ordered vortex street. The formation of this small trailing edge vortex itself is due to the higher rate of rotation at the two ends of the stroke which are required in order to pitch the airfoil from an angle of  $0^\circ$  to  $60^\circ$ .

Figure 3(iii) shows a sequence of vorticity plots for  $\alpha_a = 75^\circ$  and these plots indicate a behavior that is different for either of the two previous cases. No vortex street is observed to form in this case. Instead, one pair of counter-rotating vortices are formed in each half stroke and these vortex pairs are found to move primarily in the horizontal (right or left depending on which half of the stroke forms the vortices) direction. The key difference here is the formation of a strong and distinct trailing edge vortex that is due to the even higher rotation experienced by the airfoil at each end of the stroke. No amalgamation of the stall and trailing edge vortices is observed. Instead the stall vortex convects past the trailing edge before the trailing edge begins to form and pairs with the counter-rotating trailing edge vortex from the previous half-stroke. The trailing edge vortex from the current stroke forms subsequently and eventually pairs with the stall vortex from the following half-stroke. Thus, each vortex pair comprises of a stall vortex and a trailing edge vortex formed in two separate half-strokes. The flow is also found to be asymmetrical about  $x=0$  although this asymmetry is not as obvious as that for  $\alpha_a = 60^\circ$ .

The vortex topology is intimately linked with the aerodynamic forces experienced by the foil. Here we have computed the vertical (thrust) and horizontal (side) force coefficients by normalizing the respective forces by  $0.5\rho V_{\max}^2 c$  and it is found that the mean thrust coefficients for  $\alpha_a = 45^\circ, 60^\circ$  and  $75^\circ$  are equal to 1.07, 0.63 and 0.15 respectively. Thus, the case with the well organized inverse Karman vortex street produces the largest thrust and this is inline with previous observations (Freymuth 1990, Triantafyllou et al. 1991). A simple measure of the propulsive efficiency is the ratio of the mean thrust to the root mean square side-force and this is estimated from the current computations to be equal to 0.39, 0.31 and 0.08 for  $\alpha_a = 45^\circ, 60^\circ$  and  $75^\circ$  respectively. Thus, the case where the inverse Karman vortex street is formed produces the most thrust and does so with the highest efficiency. Thus, as concluded previously by other researchers (Freymuth 1991, Triantafyllou et al. 1991, Anderson et al. 1998), the formation of the inverse Karman vortex street coincides with optimal thrust generation for a flapping foil.

#### Paired Wing

Insects such as dragonflies and damselflies are endowed two pairs of wings wherein each pair can flap independently of the other. Various experimental studies have noted the phase relationship between the hind and forewings of these insects

(Alexander 1986, Wakeling & Ellington 1997, Azuma 1992) and attempted to explore the aerodynamic advantage that the interaction between the two wings would bestow on these insects. It is particularly interesting to study the aerodynamics of paired wings from the point of view of mimicking insect flight in a mechanical systems since in principle, paired (or even higher number) wing systems could be incorporated by a simple repetition of a single wing system. Nature seems to have limited wing systems to only a few number of pairs but there is no reason why such a limitation be imposed on mechanical systems!

In the current study we examine the aerodynamics of a paired wing in normal hover conditions. Thus, in effect another wing is added beneath the wing employed in the single wing simulations. The hindwing oscillates with the same amplitude and frequency as the forewing and the distance between the centers of the two wings is fixed to  $1.5c$ . Furthermore, the maximum pitch angle for both wings is also maintained at  $45^\circ$  and here we focus primarily on the effect of varying the phase lag of the hindwing on the aerodynamic performance of the wing pair.

Four different values of phase lag, ( $0^\circ, 90^\circ, 180^\circ$  and  $270^\circ$ ) are employed and Figure 4 shows the vorticity contour plots at one time instant for each of these cases. All cases show a highly complex interaction between vortex structures generated by the two wings and no clear vortex arrangement can be discerned. The aerodynamic performance of the paired wing system has been summarized in Figure 5. In Figure 5(a) is plotted the mean thrust coefficient for both the wings for the four different phase lags. Also, indicated on this plot is the thrust coefficient for a single wing at the same operational conditions. From this plot it is observed that both wings produce a higher than nominal thrust when the phase lag is zero. Interestingly, it has been suggested (Alexander 1984, 1986, Ruppel 1989) that parallel stroking (i.e. stroking with near zero phase lag) in dragonflies may produce higher lift forces and the current results certainly support these suggestions.

As the phase lag is increased, the thrust of the forewing decreases monotonically to a value slightly lower than the nominal value. In contrast, for the hindwing, the thrust initially increases with increasing phase lag and then decreases rapidly to a value significantly less than the nominal value. The variation of rms side force with phase lag is shown in Figure 5(b). For the fore wing, the side force is not very different from that of a single wing. However for the hind wing, the side force is more than twice the nominal value at low phase lag and remains higher than the nominal value for all values of phase lag simulated here.

The thrust efficiency for the two wings is plotted in Figure 5(c) and this again indicates that the efficiency of the forewing is similar to that observed for a single wing whereas the hind wing operates at significantly reduced efficiency for all value of phase lag. Thus the limited set of simulations presented here indicate that the overall efficiency of the paired wing system is lower than a single wing for all values of phase lag.

#### 4. CONCLUSIONS

Numerical simulations have been used to simulate and analyze the aerodynamics of flapping flight. Both single as well as paired wings have been analyzed in the normal hovering mode. For the single wing, the simulations indicate that among all the various vortex topologies associated with a flapping foil, the formation of an inverse Karman vortex street is accompanied with the highest thrust efficiency. The aerodynamic performance of a paired wing has also been examined using numerical simulations. The simulations indicate that parallel stroking produces a relatively large thrust force and this is in line with previous experimental studies. However the simulations also indicate that the efficiency of the paired wing system is lower than an isolated wing at least in the regime covered in the present study. The results presented in this paper are a precursor to a more comprehensive study of the paired wing wherein the effect of varying other parameters will be considered.

#### ACKNOWLEDGEMENT

The authors would like to acknowledge the assistance of Mr. Jason Rainer in this study.

#### REFERENCES

- Alexander, D.E. (1984) Unusual phase relationship between the forewings and hindwings in flying dragonflies. *J. Exp. Bio.*, 109, 379-383.
- Alexander, D.E. (1986) Wind tunnel studies of turns by flying dragonflies. *J. Exp. Bio.* 122, 81-98.
- Anderson, J.M., Streitlien, K., D.S. Barrett, D.S. and Triantafyllou, M.S. (1998) Oscillating Foils of High Propulsive Efficiency. *J. Fluid Mech.*, 360, 41-72.
- Ellington, C.P. (1984) The Aerodynamics of Hovering Insect Flight. IV. Aerodynamic Mechanisms. *Phil. Tran. R. Soc. Lon.* B 305, 79-113.
- Ellington, C.P. (1999) The Novel Aerodynamics of Insect Flight: Applications to Micro-Aerial Vehicles. *J. Exp. Biol.* 202 (23), 3439-3448.
- Freythuth, P. (1990) Thrust Generation by an Airfoil in Hover Modes. *Expt. Fluids.* 9, 17-24.
- Gustafson, K. & Leben, R. (1991) Computation of Dragonfly Aerodynamics. *Comput. Phys. Comm.* 65, 121-132.
- Koochesfahani, M.M. (1989) Vortical Patterns in the Wake of an Oscillating Airfoil. *AIAA J.* Vol. 27, No. 9, 1200-1205.
- Rüppell, G. (1989) Kinematic analysis of symmetrical flight maneuvers of Odonata. *J. Exp. Bio.* 144, 13-42.
- Somps, C. and Luttses, M. (1985) Dragonfly Flight: Novel Uses of Unsteady Separated Flows. *Science* Vol. 228, 1326-1328.
- Triantafyllou, M.S., Triantafyllou, G.S. and Gopalkrishnan, R. (1991) Wake Mechanics for Thrust Generation in Oscillating Foils. *Phys. Fluids.* A 3, 2835-2837.
- Udaykumar, H. S., Mittal R., and Shyy, W. Solid-Liquid Phase Front Computations in the Sharp Interface Limit on Fixed Grids. *J. Comp. Phys.* Vol. 18, pp. 535-574 (1999).
- Udaykumar, H.S., Mittal, R., Rampunggoon, P. and Khanna, A. A Sharp Interface Cartesian Grid Method for Simulating Flow with Complex Moving Boundaries. *J. Comp. Phys.* Vol. 174, 345-380, 2001.
- Wang, Z.J. (2000) Two-Dimensional Mechanism for Insect Hovering. *Phys Rev. Lett.* 85, No. 10, 2216-2219.
- Wakeling, J.M. and Ellington, C.P. 1997 Dragonfly Flight II. Velocities, accelerations and kinematics of flapping flight. *J. Exp. Bio.* 200, 557-582
- Ye, T., Mittal, R., Udaykumar, H. S., Shyy, W., 1999. An accurate Cartesian grid method for viscous incompressible flows with complex immersed boundaries, *J. Comp. Phys.*, Vol. 156, pp. 209-240.



Figure 1. Photograph of a dragonfly

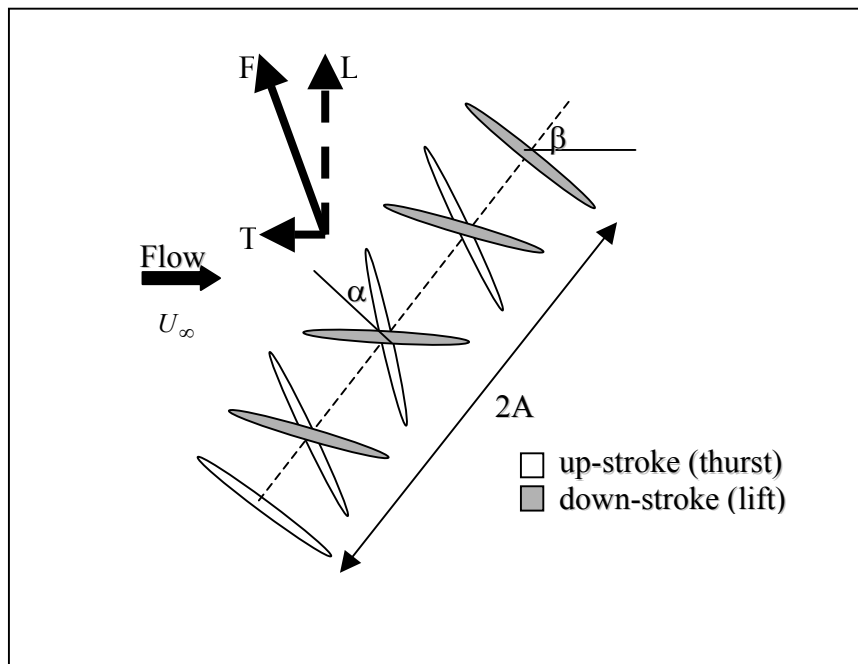


Figure 2. Schematic of a foil undergoing combined pitch-and-heave maneuver

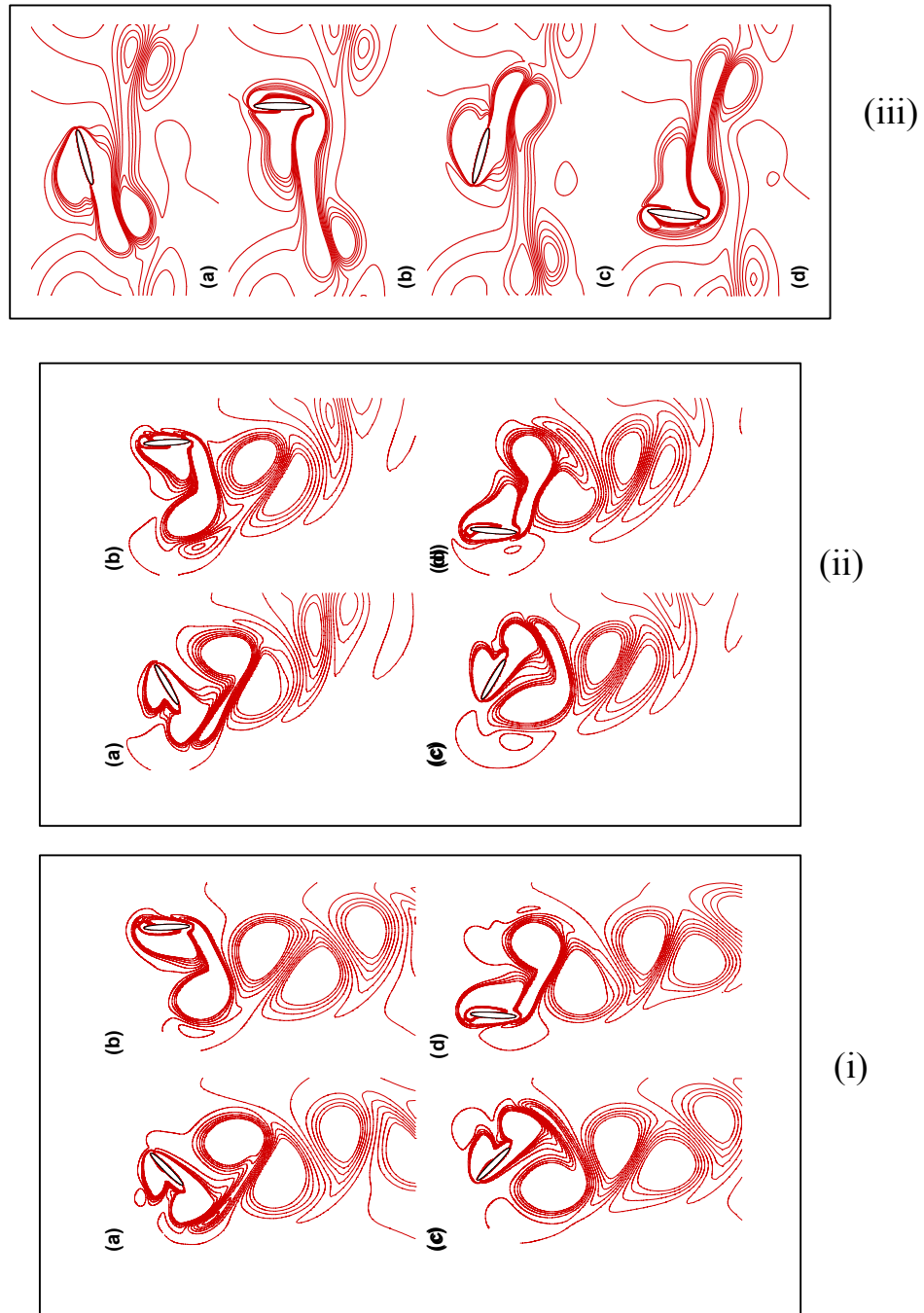


Figure 3. Sequence of spanwise vorticity contours for a single airfoil in hover.  
 (i)  $\alpha_a = 45^\circ$  (ii)  $\alpha_a = 60^\circ$  (i)  $\alpha_a = 75^\circ$

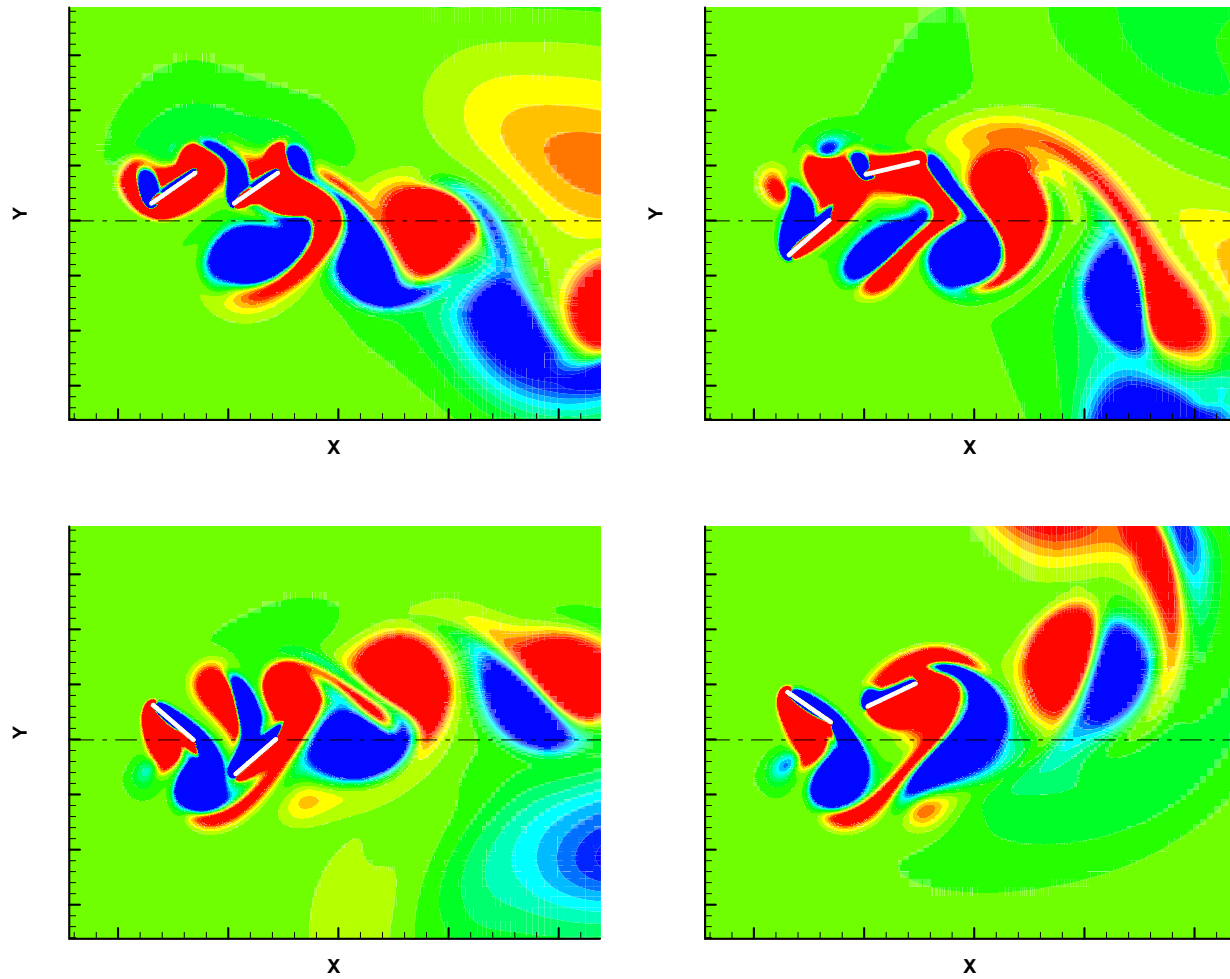


Figure 4. Spanwise vorticity contours for the paired wing with different phase lags (a)  $0^\circ$  (b)  $90^\circ$  (c)  $180^\circ$  (d)  $270^\circ$ . Note that the foils are pitching in the vertical direction (instead of horizontal). Furthermore, for the paired wing study, we employ a  $1/8^{\text{th}}$  thickness flat plate with rounded edges instead of an elliptic foil.

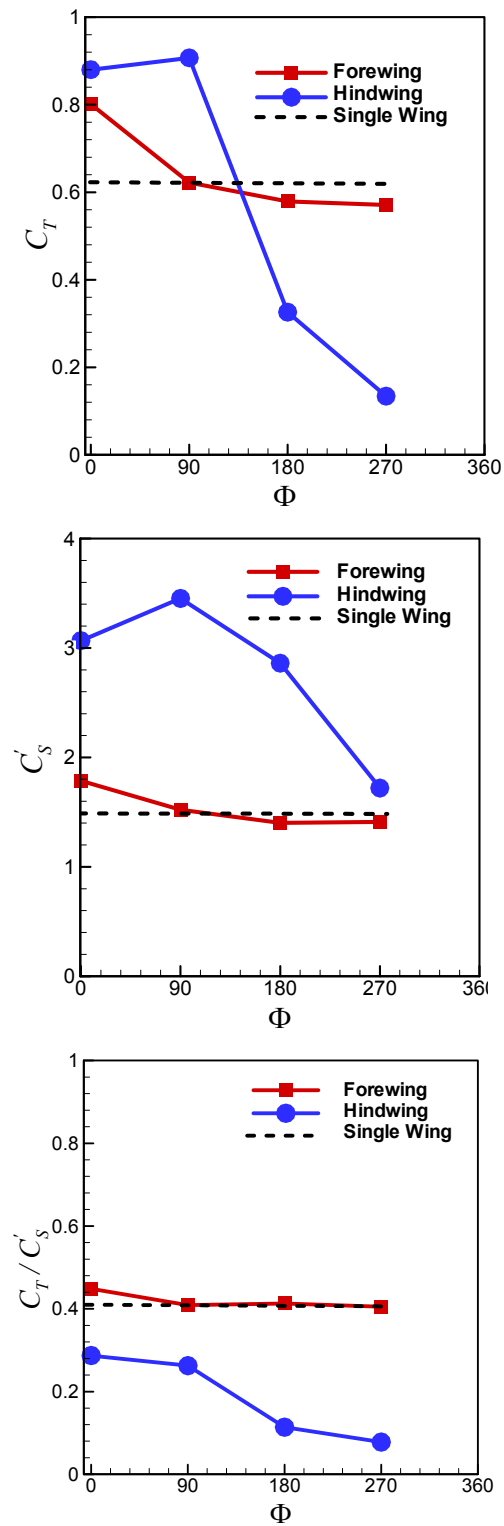


Figure 5. Aerodynamics performance of the paired wing (a) Mean thrust coefficient (b) RMS side force coefficient (c) Thrust efficiency